A Summary of the NEXT-C Flight Thruster Proto-flight Testing

Jeff Monheiser[1], Keith Goodfellow[2], Chayse Aubuchon[3], Jasper Wang[4], and Brian Ferraiuolo[5].
Aerojet Rocketdyne, Redmond, WA, 98052, USA

George Williams[6], George Soulas[7], Rohit Shastry[8], and Neil Arthur[9]
NASA Glenn Research Center, Cleveland, OH, 44135, USA

Aerojet Rocketdyne (AR), under contract to NASA Glenn Research Center, built, tested and delivered the first flight version of the NEXT-C (NASA Evolutionary Xenon Thruster – Commercial) engine system. This system is comprised of a 7 kW thruster and power processing unit which are the commercial variants of the NEXT prototype thruster and power processing unit. In addition to developing the NEXT-C engine system for potential future NASA science missions, AR is dedicated to ensuring that this propulsion system is viable for commercial users and a wider variety of commercial applications.

This paper will focus on the performance of the first flight model thruster, SN001, and presents an overview of the proto-flight testing environments and data obtained. For this first flight thruster, the proto-flight test sequence involved characterizing the performance of the thruster, in addition to vibration and thermal vacuum testing of the thruster. Between each of these environmental tests, the performance of the thruster was verified, ensuring that the environmental exposures, i.e. vibration and TVAC, did not affect the thruster performance. Specifically, the proto-flight data obtained included discharge chamber, optics and neutralizer performance. Faraday probe and ExB data obtained in the regions downstream of the thruster are presented and used to calculate thrust, and therefore specific impulse and total efficiency. Lastly, data are presented showing how the centroid of the ion beam, assumed to be indicative of the thrust vector location, varies throughout the entire proto-flight test campaign.

The proto-flight testing of the NEXT-C PPU is documented in a previously published paper by Bontempo[4]. Following the proto-flight testing of the thruster, the thruster and its PPU successfully completed a System Integrated Test (SIT) tailored to the DART Mission. After the completion of the proto-flight testing, the SN001 thruster and SN002 PPU were delivered to APL for use on the DART mission.

I. Nomenclature

APL = Applied Physics Laboratory
AR = Aerojet Rocketdyne

[1] Principal Engineer, Component Product Engineering
[2] Chief Engineer, Space Systems Chief Engineer, AIAA Member.
[3] Associate Engineer, Component Product Engineering
[4] Senior Engineer, Project and Product Engineering
[5] Specialist Engineer, Chief, Space Advanced Programs, Chief Engineering
[6] Research Engineer, Electric Propulsion Systems Branch, AIAA Associate Fellow
[7] Research Engineer, Electric Propulsion Systems Branch, AIAA Senior Member
[8] Research Engineer, Electric Propulsion Systems Branch, AIAA Member
[9] Research Engineer, Vantage Partners, Ltd., Electric Propulsion Systems Branch, AIAA Member

CoV = Coefficient of Variation, %
DART = Double Asteroid Redirection Test
DEV-C = Development Thruster – Commercial
ε = Total Efficiency,%
E_d = Discharge Losses, W/A
EFT = Electrical Functional Test
ETL = Extended Throttle Level
FOD = Foreign Object Debris
FuT = Functional Test
F_t = Thrust losses due to Beam Divergence
GRC = Glenn Research Center
I_{sp} = Specific Impulse, sec
J^{++}/J^{+} = Double to Single Ion Ratio, %
J_a = Impingement Current, mA
J_b = Beam Current, A
$j_{b\text{-}pk}$ = Peak Beam Ion Current Density, mA/cm^2
J_d = Discharge Current, A
JPL = Jet Propulsion Laboratory
$\Delta\dot{m}$ = Neutralizer Spot-To-Plume Mode Flow Margin, sccm Xe
NEXT = NASA Evolutionary Xenon Thruster
NEXT-C = NASA Evolutionary Xenon Thruster – Commercial
PaT = Performance Acceptance Test
P_{input} = Total Input Power, kW
PM1R = Prototype Thruster, first revision.
PPU = Power Processing Unit
Ref. = Reference
Req. = Requirement
SDL = Structural Dynamics Laboratory
SIT = System Integrated Test.
SN = Serial Number
STE = Special Test Equipment
T = Thrust, mN
TL = Throttle Level
TVAC = Thermal Vacuum Test
V_b = Beam Voltage, V
V_d = Discharge Voltage, V
V_{dk} = Discharge Keeper Voltage, V
V_{nk} = Neutralizer Keeper Voltage, V
V_g = Coupling Voltage, V
ΔV_t = Perveance Margin, V
V_{eb} = Electron Backstreaming Margin, V
VF = Vacuum Facility
X = Coordinate Direction
Y = Coordinate Direction

II.NEXT Program Overview

The NEXT ion propulsion system development began in 2002[1] when NASA identified a need for an ion thruster with higher power and throughput capabilities than were available. Specifically, missions being proposed required higher power levels, 5 to 10 kW, and larger propellant throughput. To satisfy this need, the NEXT ion thruster system was designed to operate up to 6.85 kW, an I_{sp} from 1400 to 4160 seconds, and thrust levels from 25 mN to 235 mN. The completion of the initial development program culminated with the production of a proto-type ion thruster system consisting of a prototype ion thruster, a prototype power-processing unit and a prototype, propellant management system[2]. This entire system was subjected to a limited environmental testing campaign and in addition, the thruster element was operated for a short duration (1680 hour) wear test[3] to ensure its operation was consistent with previous engineering model thrusters.

In an attempt to widen the market possibilities for the NEXT ion thruster system, in 2015 NASA created the NEXT-C program with the goal of advancing the technology from TRL 5/6 to TRL 8. A secondary goal for this new program was to make the NEXT ion engine more commercially attractive for other commercial interests. In contrast to the previous technology development program, the NEXT-C effort was limited in scope to only advancing the TRL of the ion thruster and the PPU, collectively referred to as the ion engine system. This new effort generated flight released drawings and delivered a flight version of the thruster and PPU. This paper covers the design and testing of the flight thruster while Bontempo[4] covers the design and testing of the PPU.

The NEXT-C ion engine system produced under the NEXT-C contact is being used for the NASA's Double Asteroid Redirection Test (DART) mission[5]. Launching in late 2021to early 2022, this mission involves impacting the smaller of a co-orbiting binary asteroid, Dimorphos, in October 2022 with a >300 kg spacecraft. The goal is to demonstrate and characterize the deflection of a hazardous asteroid with the momentum transfer from a very high speed impact by the spacecraft. By impacting the smaller, 150m asteroid and monitoring the change in its orbit around the 800m partner, it will be possible to characterize the deflection much more precisely than to detect the change in the heliocentric orbit of a single asteroid. The flight thruster and PPU have both successfully completed component and system level testing and have been integrated onto the spacecraft.

III. Thruster build description

A. Major elements

Identical to the majority of gridded ion thrusters, the NEXT-C thruster is comprised of five major elements:

- The discharge chamber, used to create the plasma from which the ions are extracted.
- The main discharge cathode, which provides energetic electrons that ionize the xenon propellant
- The ion optics, which focus and accelerate the ions forming the beam
- The neutralizer, which provides elections that charge neutralize the ion beam and prevent the charging of the spacecraft
- Plasma shield, used to prevent ambient plasma electrons from reaching screen potential surfaces.

Figure 1 is a depiction of all the elements of the thruster. In this figure, the front mask, neutralizer & gimbal mounts, the insulation panels and the plasma shield collectively make up the plasma screen assembly. Prior to NEXT-C, as mentioned previously, there had been a significant amount of testing involved in the development of the engineering model thruster. From there, the design evolved making it more flight-like and able to survive both the launch vibration and thermal environments. At the completion of that effort, a complete set of development level drawings were created from which the PM1 thruster was built. This prototype thruster was subjected to both random vibration and thermal vacuum tests[6]. Based upon the results of that testing, a few minor design changes were made and retrofitted to the existing hardware to produce PM1R. The PM1R thruster was then subjected to a wide variety of development tests to completely characterize its performance over a wide variety of operating points.

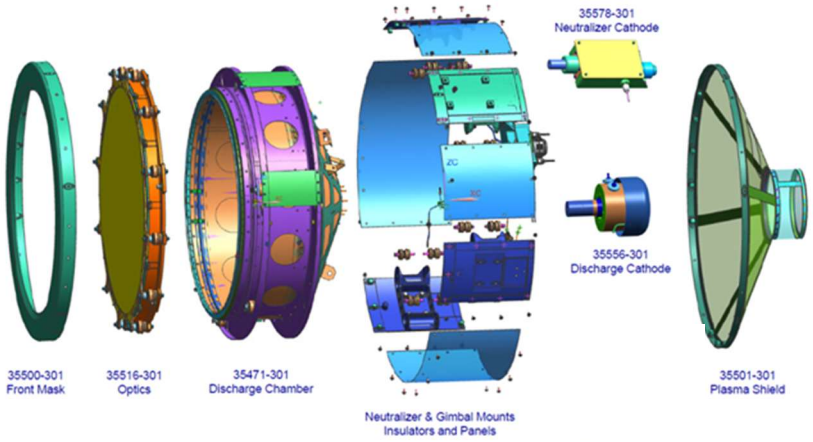

Figure 1 A graphical depiction of the major elements associated with the NEXT-C ion thruster.

To support future NASA missions, the NEXT-C program was tasked with producing a complete flight-ready design and released set of production drawings from which flight thrusters could be built. To expand the potential

market for the flight thrusters, design changes were made resulting in a more commercially producible thruster. These changes were integrated into the PM1R thruster, creating the DEV-C thruster. Specifically, the following changes were implemented.

1. Discharge Chamber

For the discharge chamber, the majority of the design changes involved process improvements which both reduced the number of hours required to assemble the thruster and limit the amount of FOD introduced to the assembly during manufacturing. In addition, some changes were implemented in the gimbal and neutralizer mounts to improve the fitment of the plasma shields making the final assembly of the thruster easier. Lastly, tooling embosses were added to the gimbal mounts, facilitating the addition of a handling ring and optics cover. Both of these greatly simplify and protect the thruster during spacecraft integration.

2. Discharge Cathode

Using additional thermal data collected during early development testing, the thermomechanical analysis originally developed for PM1R was refined and a new analyses were performed. These new analyses revealed two concerns. The first concern was easily remedied by changing the material for the discharge cathode mount to a nickel alloy. The second concern is the use of two dissimilar materials within the discharge cathode assembly creates a potential fatigue concern as the thruster temperature varies between the high and low temperature extremes listed in the product specification. This concern was analyzed for the DART mission and found to be an acceptably low risk.

3. Neutralizer

To improve the manufacturability of the neutralizer, the internals of the design were changed slightly in that the locations of the expellant input and the electrical harness were switched.

4. Optics

Associated with the ion optics, the majority of the effort in this program was directed at documenting and releasing the processes for manufacturing and subsequent alignment of the optics. While developing the process for the alignment, it was found that the locations of the screen grid holes relative to the accel grid holes were slightly different from those measured on previous generations of engineering model optics. Specifically for this set of flight ion optics, the accelerator grid holes were slightly shifted in the radial direction. The relative locations of the screen to accelerator grid holes is controlled by the compensation factor. However for this particular grid set, the same compensation factor used for PM1R resulted in apertures that were slightly shifted radially. This difference between the expected location and the actual location is referred to as the radial misalignment of the optics. As would be expected, this radial misalignment has a strong effect on the perveance limits for the optics set and as will be shown, these limits for this flight set of optics was indeed lower than previous prototype optics. The lower perveance limits do prevent this thruster from operating at the lower throttle levels, which are not required for the DART mission. So while the radial misalignment does limit the thruster operation, there is still plenty of perveance margin for the DART mission.

A new manufacturing process has been developed and demonstrated to eliminate the radial misalignment in future ion optics. Because the DART mission did not require operation beyond the pervevance limits of the delivered optics, the flight thruster optics were not updated using the new manufacturing process. All future ion engine systems delivered by AR will use this new manufacturing process and be capable of operating over the entire NEXT-C throttle range[7].

IV.Experimental Setup

The performance of the flight thruster was determined by measuring the electrical characteristics of the thruster at each operating point. These measurements, along with characteristics of the ion beam plasma, were used to compute the thrust and specific impulse at each operating condition. A probe diagnostic suite manufactured by Plasma Controls, LLC, under contract from AR, was used to measure the beam plasma characteristics. Specifically, this diagnostics suite utilized three Faraday probes, an ExB probe and a thrust vector probe located at the far end of the vacuum facility.

Presented in Figure 2 is the entire experimental setup constructed by AR and installed within Vacuum Facility 6 (VF-6) at NASA Glenn Research Center (GRC). As shown on the sketch, the plasma diagnostics suite is comprised of a far-field actuator on which a far-field Faraday probe is mounted, a thermal shroud (referred to simply as the shroud), a mounting structure for the flight thruster, a mid-field probe suite along with motion stages for the probes. The mid-field probe suite, pictured on Figure 3, contains a near-field Faraday probe located 4.5 cm downstream of the accelerator grid, a mid-field Faraday an **E**x**B** probe located 82 cm downstream of the accelerator grid. The motion stages, on which these probes are mounted, have been programed to move the mid-field Faraday probe in an arc about

the center of curvature for the ion optics. Similarly, the stages were programed to move the near-field Faraday probe in a straight line 4.5 cm downstream of the accel grid. In addition to these three Faraday probes, a single **E**x**B** probe was located on the mid-field probe suite and data were obtained 82 cm downstream of the accelerator grid. The **E**x**B** probe included a collimator that sampled beam ions from a 1.84 cm diameter spot emanating from the thruster accelerator grid. Identical to the mid-field Faraday probe, the probe motion was an arc centered on the center of curvature of the ion optics.

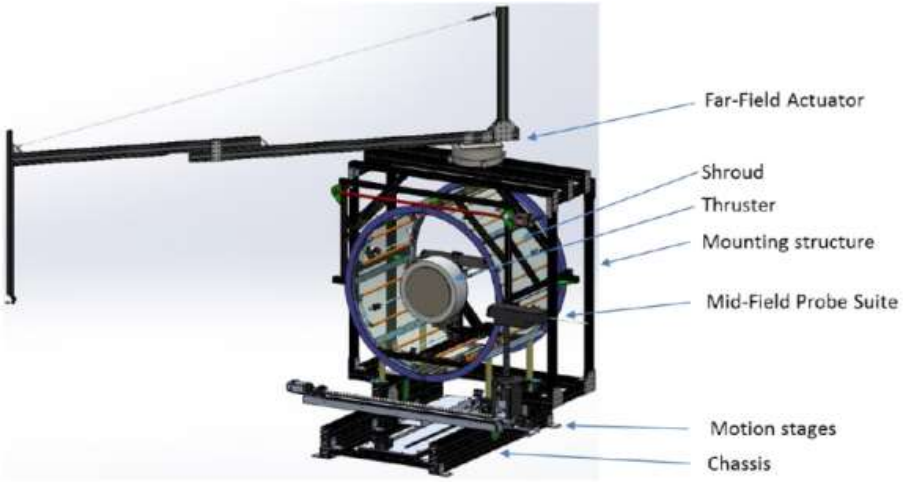

Figure 2 A sketch of the experimental test setup used to perform the proto-flight testing of the SN 001 thruster.

The far-field actuator is a rotary stage with a long boom on the end of which a Faraday probe is located. This far-field Faraday probe is located 2.7 m downstream of the accelerator grid.

Consistent with the procedure presented by Pollard et. al.[8], the data obtained from these probes are used to calculate thrust for the slight variations in the ion beam divergence and composition. Specifically the far-field probe data measured 2.7 meters downstream was used to correct the thrust for the beam divergence and the ExB probe data along with the near-field probe data are used to correct for the fraction of double to single ions within the ion beam.

In addition to the four plasma probes described above, the thrust vector probe pictured on Figure 4 was installed for all the testing conducted. This probe is similar in design to the probe developed by JPL and used to measure the thrust vector for the NSTAR thruster[9]. In contrast to the NSTAR probe, this larger probe has 16 vertical and horizontal rods, and the outside dimension of the array is 2.54 m on a side. For the data to be presented, the array was located 12.4 m downstream of the thruster and based upon the probe size and axial location, the probe has an acceptance half angle of ~6 degrees.

The thermal vacuum cycle testing performed utilized the thermal shroud pictured on Figure 5. This shroud can be both cooled using liquid nitrogen and heated using quartz lamps. To reduce the radiant heat absorbed by the thruster during the cold soak portions of the test, a retractable curtain on the downstream opening of the shroud was lowered during these non-firing periods. Also shown on the picture is the proto-type thruster installed on the shroud centerline near the downstream plan of the shroud.

All the results to be presented were obtained at the NASA GRC using test equipment and tooling developed, owned and provided by AR. All the hot fire performance data were obtained in VF6 and the vibration testing was performed at the Structural Dynamics Laboratory (SDL) at NASA GRC.

Lastly, presented on Figure 5 is the coordinate system used for all the firing data to be presented. For all the data obtained during the firing of the thruster, the "thruster" coordinate system is used to present the data. For this coordinate system, as suggested by the picture, the origin is located at the center of the accelerator grid, tangent to the dome of the grid. The Y-direction points through the neutralizer and the Z-direction is the thrust direction. Lastly, when looking from the upstream direction back at the thruster, the X-direction is to the right when the thruster is mounted with the neutralizer straight up.

Figure 3 A picture of the Mid-field probe suite containing the probes used to make the ion beam measurements.

V.Thruster Proto-flight Testing

A. Test program description

Following typical testing protocols, the flight thruster (SN001) was tested to proto-flight levels using the sequence shown on Figure 6. As shown on the figure, the proto-flight testing began by subjecting the thruster to an initial performance assessment test, PaT. The purpose of this test was to determine the baseline performance of the thruster from which a comparison to previous hardware could be performed. Lastly, for this PaT, the thruster input power was varied from 1.1 kW, TL05, up to 6.4 kW, TL40. However, because this thruster was delivered to APL for use on the DART mission, this initial PaT test was the only time the thruster was operated at throttle levels higher than TL29.

At the completion of the initial PaT, the thruster was then vibration tested to proto-flight levels. As is customary for proto-flight applications, the flight thruster was not subjected to a shock test. Instead, a lower fidelity version of the flight thruster (labeled DEV-C) was shock tested and a similarity analysis performed to demonstrate applicably to the flight thruster.

After the vibration test, the thruster was installed within the aforementioned thermal shroud. Once the thruster was installed, a functional test, FuT #1, was conducted in which the performance of the thruster was measured at only operating conditions TL28, TL29, and ETL2.7A along with a 1.1 kW operating condition (TL05). At the completion of the FuT #1, the thruster was subjected to a thermal vacuum test in which its temperature was varied from proto-flight cold to hot for three cycles. At the completion of the TVAC testing, the final performance of the thruster was then measured during the last abbreviated functional test, FuT #2. This test sequence serves to verify the performance of the thruster has not changed after each major environmental test. To that end, as indicated on Figure 6, at the completion of each individual test, an electrical functional test was performed to verify that the impedances of all the thruster elements had not changed since the previous measurements.

Figure 4 A picture of the thrust vector probe located at the downstream end of VF 6

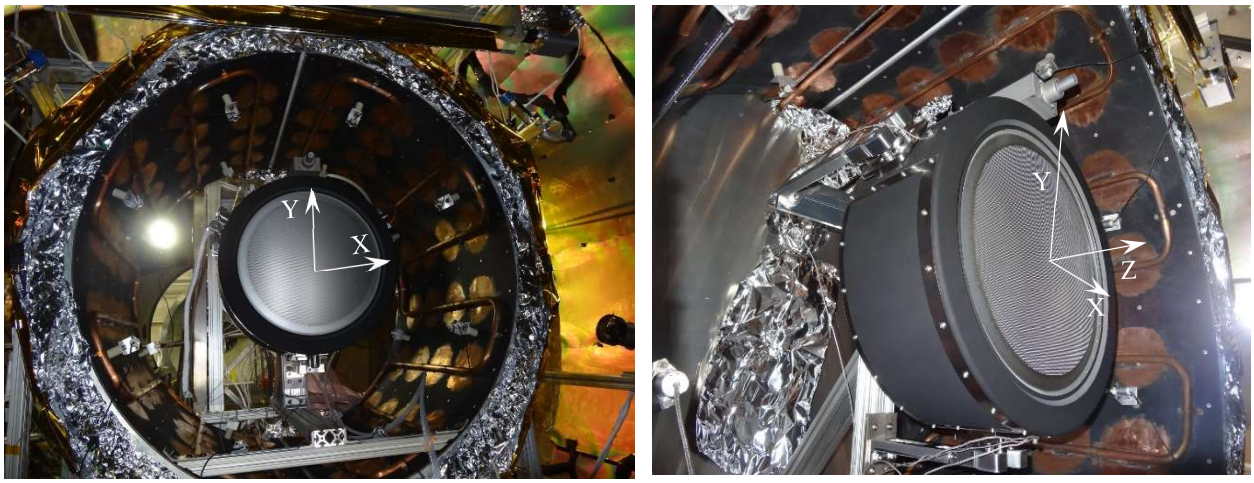

Figure 5 Pictures of the flight NEXT-C thruster mounted within the thermal shroud used to perform the TVAC testing.

At the completion of the proto-flight testing outlined on the figure, the thruster was mated with the flight power processing unit and a system integrated test (SIT) was performed. Results from that testing were discussed elsewhere[10], and showed no concerns or changes in the system performance.

B. Flight thruster performance results

As indicated previously, the first thruster test measured its initial performance. Based upon the AR, NASA and APL agreed upon test plan, the initial performance of the thruster was measured at a select number of total NEXT throttle levels[7] consistent with previously tested thrusters. Specifically, performance data were measured at TL40, TL37, TL29, TL28, ETL2.7A, TL09, TL05, TL01, and Diode Mode. However, due to the radial misalignment of the ion optics, mentioned previously, the technical team, including APL, decided that since the thruster was to be used on the DART mission, the added risk associated with obtaining the TL01 performance data point was greater than the benefit of the data and would therefore be dropped from the initial PaT testing.

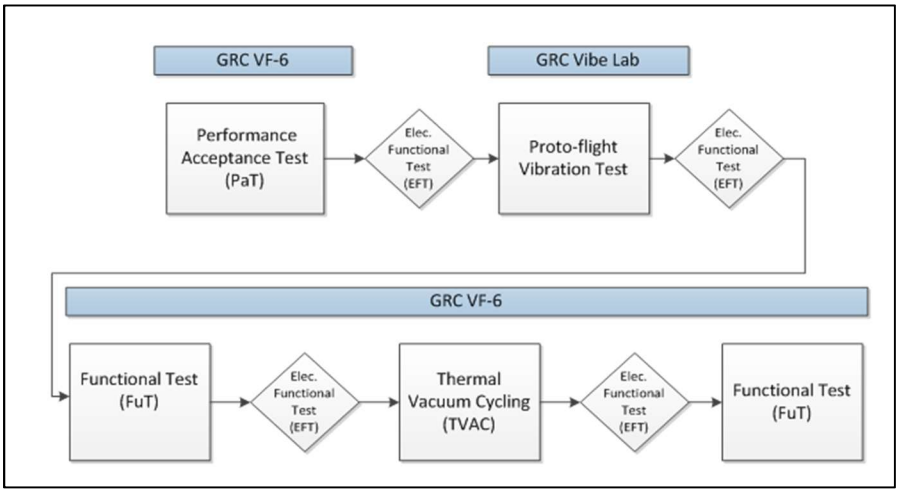

Figure 6 Testing protocol for the flight thruster. The testing follows the typical test like you fly pattern.

Presented on Table 1 are the performance values measured for the flight thruster as the total input power was varied from 1.1 kW to 6.8 kW. A comparison to reference values obtained on similar hardware was completed and it confirmed that the performance the flight thruster was similar to prior NEXT thrusters.

This comparison with the data of Table 1, showed that the performance values for total input power and thrust were very slightly lower than the maximum power measured on the previous hardware. The next two rows on the table show the specific impulse and total thruster efficiency which were slightly higher than the comparison values. From the data presented on this table, the thruster performance was determined to be within the small family of comparable thrusters making it acceptable for use on the DART mission.

Table 1 Performance values measured during the initial PaT for the flight thruster.

TL:	**TL40**	**TL37**	**TL29**	**TL28**	**TL09**	**TL05**
J_b, V_b:	**3.52 A, 1800 V**	**3.52 A, 1179 V**	**2.70 A, 1179 V**	**2.70 A, 1021 V**	**1.20 A, 1179 V**	**1.20 A, 679 V**
Performance	**PaT**	**PaT**	**PaT**	**PaT**	**PaT**	**PaT**
P_{input}, kW	6.833	4.694	3.619	3.213	1.700	1.119
T, mN	233.6	192.1	146.7	137.5	63.8	48.9
I_{sp}, s	4150	3410	3365	3153	3190	2443
E	0.695	0.684	0.669	0.662	0.587	0.523

In addition to the thruster performance present on Table 1, during the PaT, detailed performance measurements of the individual thruster components were measured and compared to the family of data. Presented on Table 2 are the discharge chamber performance parameters. The comparison of this data and the family data showed good consistency with the following slight differences. For the flight thruster, the discharge voltage was typically about a volt greater than the family values. In addition, the comparison showed that while the discharge voltage was slightly higher than the comparison data, the discharge current was lower. Because of this, the discharge losses, $E_b = \frac{(J_d * V_d)}{J_b}$, were lower than the family data for all the throttle levels tested. This indicates that although the discharge voltages were slightly

higher for the flight thruster, the discharge losses were as expected indicating that the discharge chamber performance is comparable to prior NEXT thrusters.

Table 2 Discharge Chamber Performance.

TL:	TL40	TL37	TL29	TL28	TL09	TL05
Jb, Vb:	3.52 A, 1800 V	3.52 A, 1179 V	2.70 A, 1179 V	2.70 A, 1021 V	1.20 A, 1179 V	1.20 A, 679 V
Discharge	**PaT**	**PaT**	**PaT**	**PaT**	**PaT**	**PaT**
J_d, A	17.60	19.27	15.58	16.08	8.20	9.00
V_d, V	24.41	25.48	25.13	25.32	28.73	28.87
V_{dk}, V	5.72	6.02	5.71	5.71	4.64	4.73
E_d, W/A	122.1	139.5	145.1	150.7	196.4	214.0
J++/J+, %	4.37	5.18	4.83	4.95	8.20	7.84

Table 3 presents the neutralizer performance data for the six throttle levels tested which was again compared to reference values measured on various previous neutralizers having similar geometries. The comparison showed that, with the exception of the neutralizer flow margin at TL29 and TL09, the neutralizer performed comparable to the reference hardware. For these two throttle levels, the difference between the measured and the comparison value were very similar in magnitude to the resolution of the measurement technique, hence the differences are likely due to the resolution of the measurement technique.

Table 3 Neutralizer Performance Values.

TL:	TL40	TL37	TL29	TL28	TL09	TL05
J_b, V_b:	3.52 A, 1800 V	3.52 A, 1179 V	2.70 A, 1179 V	2.70 A, 1021 V	1.20 A, 1179 V	1.20 A, 679 V
Neutralizer	PaT	PaT	PaT	PaT	PaT	PaT
V_{nk}, V	11.78	11.27	12.11	12.12	15.14	15.18
V_g, V	-11.44	-11.02	-11.20	-11.14	-10.21	-10.21
$\Delta\dot{m}$, sccm	1.90		1.49		0.69	

Presented on Table 4 are the performance data obtained for the ion optics for SN001. Shown are the values measured during the PaT and the family value for comparison. The perveance margin values are lower than those measured on previous prototype type optics sets due to the radial misalignment described previously. For the electron backstreaming limit, and the thrust correction factor, the values measured are slightly out of family with the reference values. The reason for the discrepancies is due to the very limited data sets for the reference data and the fact that these values did not have any margin added to them.

Table 4 Optics Performance data.

TL:	TL40	TL37	TL29	TL28	TL09	TL05
J_b, V_b:	3.52 A, 1800 V	3.52 A, 1179 V	2.70 A, 1179 V	2.70 A, 1021 V	1.20 A, 1179 V	1.20 A, 679 V
Optics	**PaT**	**PaT**	**PaT**	**PaT**	**PaT**	**PaT**
J_a, mA	15.30	13.66	8.98	9.50	3.33	2.89
ΔV_t, V	892		1010		1267	
V_{eb}, V	-177.5	-138.4	-123.8	-109.4	-86.6	-55.4
F_t	0.9630	0.9728	0.9691	0.9603	0.9619	0.9756
$j_{b\text{-}pk}$, mA/cm2	4.745	4.829	3.763	3.774	1.85	1.847

As shown on Figure 6, after each of the environmental tests, a functional test was performed. As mentioned previously, the functional tests (FuT) measured the performance of the thruster at only TL29, TL28, ETL2.7A and TL05 throttle levels after each environmental test. As such, the first FuT was conducted after the vibration test and

the second was conducted at the completion of the thermal vacuum testing. The data from these two FuT tests were then compared to those data obtained during the initial PaT to see if there were any changes in the thruster operation that may have been caused by either vibration or TVAC testing.

Table 5 contains the performance data computed for the throttle levels TL29, TL28, and ETL2.7A, as well as, TL05. Presented on the table are the total input power for the thruster, the computed thrust and specific impulse and total thruster efficiencies. In addition, for each parameter, the average of the three measurements and the coefficient of variation (CoV) are presented as a measure of the variability in the three measurements. Lastly, for the throttle levels of TL29, TL28, ETL2.7A and TL05, the same reference values discussed previously were used for a comparison to the data. Reviewing the table shows that for the TL29, TL28, and ETL2.7A conditions, the CoV for the input power is less than 0.20% showing very good agreement between the values. Similarly, for the thrust, specific impulse and efficiency, the highest CoV is 1.4% for the efficiency which shows good agreement between the tests. For the TL05 data, the highest CoV is less than 1% which again shows very good agreement between the three tests at this operating condition. This observation suggests that neither the vibration nor the TVAC testing affected the operation of the thruster.

Table 5 A comparison of the initial thruster performance to that measured after both vibration and TVAC testing.

TL:	TL29				TL28				ETL2.7A				TL05			
J_b, V_b:	2.70 A, 1179 V				2.70 A, 1021 V				2.70 A, 936 V				1.20 A, 679 V			
Perf.	**PaT**	**FuT #1**	**FuT#2**		**PaT**	**FuT#1**	**FuT#2**		**PaT**	**FuT#1**	**FuT#2**		**PaT**	**FuT#1**	**FuT#2**	
P_{input}, kW	3.62	3.63	3.63		3.21	3.21	3.22		2.99	2.99	2.99		1.12	1.13	1.13	
	Ave=	3.627	CoV=	0.20%	Ave=	3.213	CoV=	0.11%	Ave=	2.991	CoV=	0.10%	Ave=	1.127	CoV=	0.67%
T, mN	146.7	145.6	147.8		137.5	136.0	135.8		131.7	130.3	130.1		48.9	48.8	48.9	
	Ave=	146.7	CoV=	0.73%	Ave=	136.4	CoV=	0.68%	Ave=	130.7	CoV=	0.68%	Ave=	48.9	CoV=	0.02%
I_{sp}, s	3365	3339	3338		3153	3118	3114		3055	3022	3017		2443	2443	2443	
	Ave=	3347	CoV=	0.46%	Ave=	3128	CoV=	0.69%	Ave=	3031	CoV=	0.69%	Ave=	2443	CoV=	0.02%
E	0.669	0.657	0.656		0.662	0.647	0.645		0.660	0.646	0.643		0.523	0.519	0.516	
	Ave=	0.66	CoV=	0.61%	Ave=	0.65	CoV=	1.40%	Ave=	0.65	CoV=	1.42%	Ave=	0.52	CoV=	0.65%

Table 6 presents discharge chamber performance for the TL29, TL28 and ETL2.7A conditions, as well as, for TL05. A similar comparison between the values shows very good agreement over the three tests indicating that the environmental testing did not affect the performance of the discharge chamber.

Table 6 A comparison of the initial Discharge Chamber Performance to that measured after both vibration and TVAC testing.

TL:	TL29			TL28			ETL2.7A			TL05		
J_b, V_b:	2.70 A, 1179 V			2.70 A, 1021 V			2.70 A, 936 V			1.20 A, 679 V		
Discharge	**PaT**	**FuT#1**	**FuT#2**	**PaT**	**FuT#1**	**FuT#2**	**PaT**	**FuT#1**	**FuT#2**	**PaT**	**FuT#1**	**FuT#2**
J_d, A	15.58	15.91	16.08	16.08	16.24	16.15	16.28	16.39	16.57	9.00	8.98	8.98
V_d, V	25.13	24.59	24.83	25.32	24.90	24.98	25.41	25.13	25.43	28.87	28.76	27.41
V_{dk}, V	5.71	5.59	5.05	5.71	5.70	5.41	5.71	5.79	5.13	4.73	4.90	2.83
E_d, W/A	145.1	144.8	147.8	150.7	149.7	149.3	153.2	152.5	156.1	214.0	219.9	227.9
j_{++}/j_{+} (%)	4.83	4.65	5.30	4.95	4.74	5.40	5.27	4.87	5.53	7.83	7.95	8.16

Table 7 presents the data obtained for the neutralizer performance over the three tests. While the measured values are inconsistent with the reference values, they are extremely consistent over the three tests. This suggests that neither the vibration nor the TVAC testing had any affect upon the operation of the neutralizer.

The ion optics performance data obtained before and after the environmental testing are presented in Table 8. These data show that from the PaT to the first FuT, all the data show good agreement with the exception of the impingement current and the X location of the thrust vector. A comparison of these data shows that the impingement current increased slightly from the initial PaT and the thrust vector moved slightly in the X direction by about 10 cm, corresponding to 0.46 degrees. For the impingement current, comparing the values obtained during the first two tests with that obtained during the second FuT, shows that the impingement current decreased to the original value

measured during the first test. This increase and subsequent reduction in the impingement current between the two tests is indicative of outgassing during the initial FuT test. A review of the first thermal vacuum cycle data shows that the vacuum tank pressure and impingement current initially increased as the thermal shroud heated up, then eventually decreased to the nominal levels. This strongly suggests that the thermal shroud was outgassing during the hot portion of the initial TVAC cycle, resulting in a higher neutral density in the vicinity of the thruster leading to higher impingement currents.

Table 7 A comparison of the initial Neutralizer performance to that measured after both vibration and TVAC testing.

TL:	TL29			TL28			ETL2.7A			TL05		
J_b, V_b:	2.70 A, 1179 V			2.70 A, 1021 V			2.70 A, 936 V			1.20 A, 679 V		
Neut.	PaT	FuT#1	FuT#2	PaT	FuT#1	FuT#2	PaT	FuT#1	FuT#2	PaT	FuT#1	FuT#2
V_{nk}, V	12.11	11.93	11.57	12.12	11.94	11.84	12.33	12.18	11.85	15.18	15.08	14.26
V_g, V	-11.20	-11.02	-11.03	-11.14	-11.02	-10.98	-11.27	-11.20	-11.14	-10.21	-9.99	-9.69
$\Delta\dot{m}$, sccm	1.49	1.50	1.50							0.69	0.69	0.69

Table 8 A comparison of the ion optics data gathered over the environmental testing.

TL: Jb, Vb:	TL29 2.70 A, 1179 V			TL28 2.70 A, 1021 V			ETL2.7A 2.70 A, 936 V			TL05 1.20 A, 679 V		
Optics	PaT	FuT#1	FuT#2	PaT	FuT#1	FuT#2	PaT	FuT#1	FuT#2	PaT	FuT#1	FuT#2
Ja, mA	8.98	10.92	8.91	9.50	11.10	10.10	9.98	11.37	9.70	2.89	3.52	2.72
□Vt, V	1010	1018	999							1267	1281	1280
Veb, V	-123.8	-123.8	-122.8	-109.4	-111.8	-111.0	-99.8	-101.8	-98.8	-55.4	-54.6	-58.6
Ft	0.969	0.969	0.9670	0.960	0.961	0.974	0.974	0.975	0.975	0.976	0.975	0.975
jbpk, mA/cm2	3.763	3.728	3.723	3.774	3.764	3.776	3.811	3.762	3.789	1.847	1.785	1.862
Thrust Vector	PaT	FuT#1	FuT#2	PaT	FuT#1	FuT#2	PaT	FuT#1	FuT#2	PaT	FuT#1	FuT#2
X, cm	29.78	20.10	20.45	30.01	20.21	20.67	30.55	20.53	20.47	26.59	18.46	18.45
Y, cm	31.81	31.14	31.95	31.99	30.61	32.04	32.77	31.26	31.93	30.95	31.11	30.45

As mentioned previously, the other parameter showing a change from the initial PaT to the FuT tests is the X component of the thrust vector. Presented on Figure 7 are the thrust vector locations for four common throttle levels, TL05, ETL2.7A, TL28 and TL29. On this figure, the open symbols represent the initial data obtained during the first PaT and show the thrust vector was originally located at an X and Y location of 30 cm and 32.5 cm respectively for ETL2.7A, TL28, and TL29. For TL05, the thrust vector is located at 26.6 cm and 31 cm respectively. The thrust vector data obtained during the first FuT performed after vibration test, shown as the solid black symbols, and the data obtained during second functional test, performed after TVAC, exhibited as solid red symbols. A comparison of these three data sets shows the unexpected ten centimeter (0.46 degree), shift in the X location and a one centimeter shift in the Y location. This unexpected change in a single direction leads one to suspect an alignment error in the installation of thruster. However, the alignment of the thruster to the thrust vector probe was completed using the same procedure as the initial alignment. In addition, prior to removing the thruster at the completion of the two functional tests, the alignment of the thruster to the vector probe was re-verified and agreed with the initial alignment. Based on this result, thruster alignment had been ruled out, so the only logical explanation for the shift in the thrust vector is that during the vibration test, the optics shifted very slightly. Regardless, the shift was small (i.e. 0.46 degrees) and the thrust vector still met its requirements

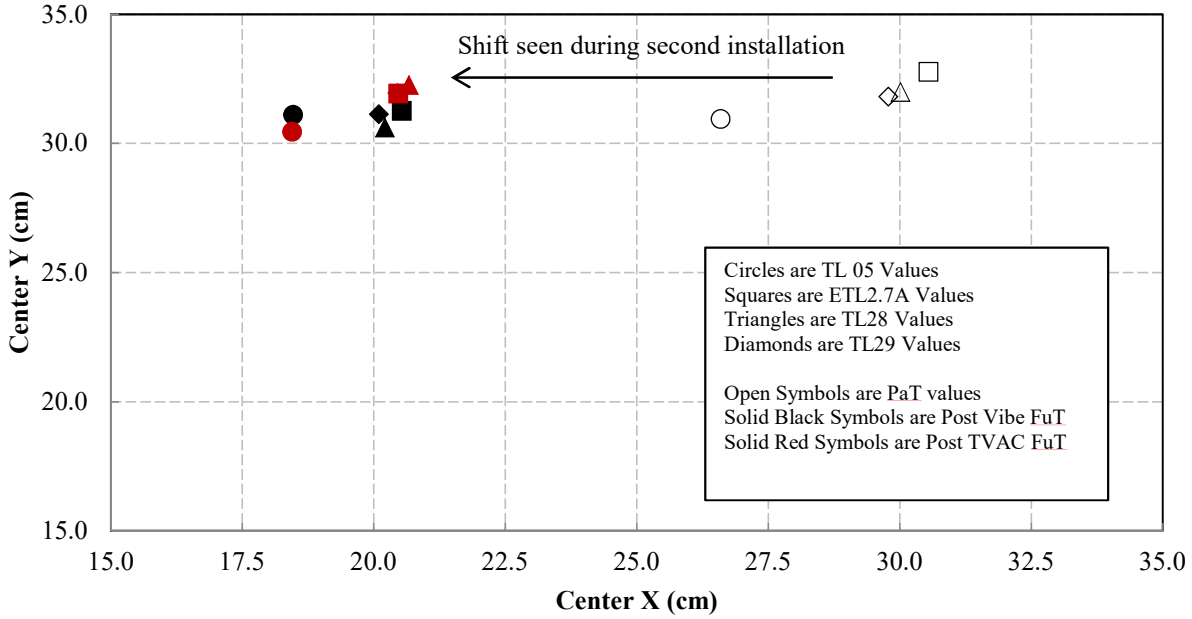

Figure 7 A comparison of the Thrust Vector locations measured of the three performance tests conducted.

Presented on Figure 8 is a plot of the X and Y beam center locations measured for all the throttle levels tested. The X and Y locations of the ion beam centroid are measured using the thrust vector probe described previously and assumed to be indicative of the thrust vector location. As shown on the figure, the X center location for the ion beam varies from 26 to 31 cm and the Y beam location varies from 28 cm to 33 cm.

In addition, presented on the figure are the discharge powers for each throttle level and consistent with measurement made by others, the thrust vector seems to be a strong function of the discharge power. This relation suggests that as the discharge power increases, the ion optics temperature increase causing movement of the ion beam. It should be noted that while the distances presented on the figure are on the order of a few tens of centimeters, the actual thrust vector angle is only a few degrees, (i.e. 1.9 to 2.0 degrees).

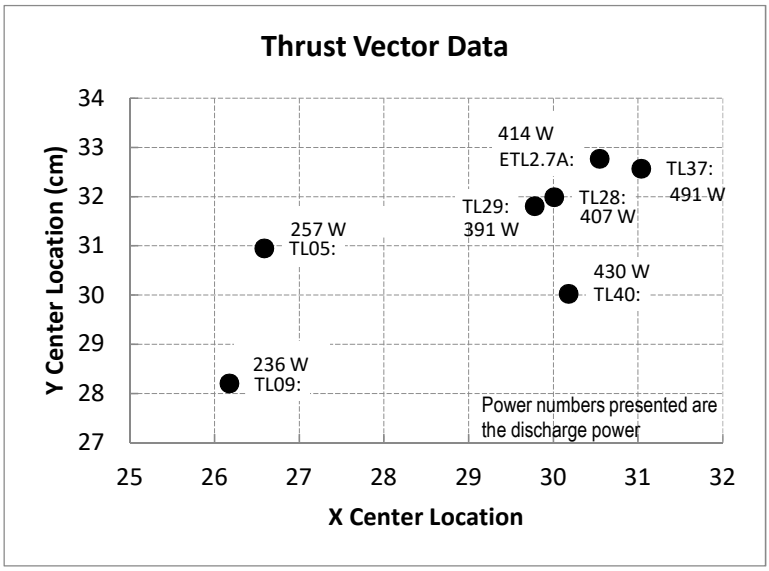

Figure 8 Thrust vector as a function of Throttle Level. Note, these data were obtained during the initial PaT.

C. Vibration

As shown on Figure 6, at the completion of the PaT testing, an electrical functional test was performed in which all the electrical impedances of the thruster components were measured to ensure no changes had been caused by the testing. After those measurements were performed, and the data reviewed confirming that no changes had occurred, the thruster was removed from VF-6 in preparation for vibration testing. As mentioned previously, the vibration testing was performed at the Structural Dynamics Laboratory at NASA GRC. The vibration testing campaign consisted of random vibration to proto-flight levels, Figure 9,

and durations. The random vibration testing was performed using a force limiting technique per NASA-STD-7004. The force limitations and methodologies were derived during previous development testing utilizing the DEV-C thruster. The procedure involved utilizing inputs from the three force transducers located at each gimbal interface to limit vibration inputs when force limits were exceeded. This can be a very complicated procedure because two of the three force transducers are not aligned with the axis of test. Lastly, during the thruster installation, a clean piece of white paper was placed between the thruster and the slip table to capture any particulates that may come from the thruster as a result of testing.

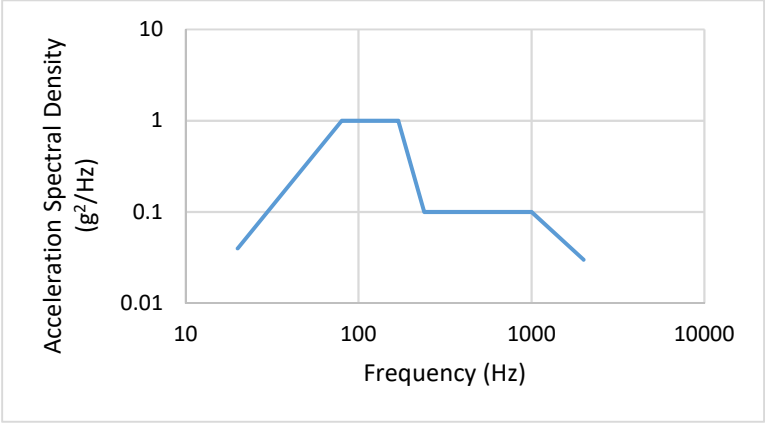

Figure 9 The NEXT-C proto-flight random vibration spectrum.

Prior to testing, a low-level sine survey was performed to document the natural frequency responses of the test article. Next, the random vibration test was performed at proto-flight levels. For each axis of random vibration testing, the vibration level was slowly ramped up to -6dB of the planned proto-flight levels to ensure the integrity of the test setup. Once the test team was satisfied with the setup, the test proceeded into full levels. After the full level proto-flight test, a second, low level sine survey was performed to verify that the fundamental frequencies of the thruster had not change as a result of the random vibration test. Once the second low-level, sine survey was completed, the sine vibration testing, from 5 to 100 Hz, was performed. Finally, a final low-level sine survey was performed to look again for shifts in the fundamental frequencies. At the completion of this test series for a single axis, an electrical functional test was performed in addition to a visual inspection of the thruster and an inspection of the paper for any debris from the thruster. Then, this test campaign was repeated for each of the remaining axes. For the X axis the total test level applied to the flight thruster was 15.97 G_{rms}. For the Y axis, the values was 15.94 G_{rms} and lastly for the Z axis the value was 14.68 G_{rms}. These values are all lower than the theoretical 16.4 G_{rms} due to the force limiting performed for each axis, and were greater than 13.94 G_{rms}.

For the sake of brevity, presented below are only the random and sine vibration data measured in the Z axis. Only these data are presented because they are in the thrust direction that includes the primary response of the ion optics. Presented on Figure 10 is a picture of the thruster mounted in the vibration fixture and oriented in the Z direction. It should be noted that for these vibration results, as pictured on the figure, the thruster was rigidly mounted to a fixture that was in turn mounted directly to the vibration table. For this testing, no gimbal was included in the test setup.

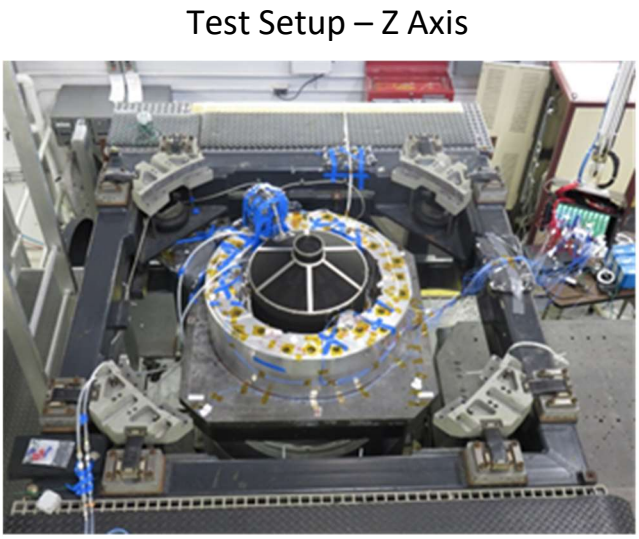

Figure 10 A picture of the flight thruster mounted on the SDL vibration table. The thruster is oriented to measure response data the Z direction.

Presented on Figure 11 are the control accelerometer response data obtained during the random vibration test. This figure shows with the exception of the first three fundamental frequencies and the very high frequencies, all the control response data are within the tolerance limits. The portions where the control responses are lower than the tolerance values is due to the force limiting procedure used to limit the input to the test. This also indicates that the first, second and third fundamental frequencies are at 211 Hz, 248 Hz, and 366 Hz, respectively, which compares very well to previous data, obtained using the DEV-C thruster.

As described previously, both before and after the random vibration test, and before and after the sine vibration test, a low-level, sine survey was performed to characterize any shifts that may have occurred during the two, vibration tests. Shown on Figure 12 is a

comparison of the data obtained for the neutralizer enclosure before (blue) and after (red) the random vibration and after (green) the sine vibration test. The figure shows that after each of the tests, there was a negligible change in the response of the neutralizer enclosure. This lack of a shift in the response data indicates that no damage occurred during either of the two vibration tests. In addition to sine response data for the neutralizer, the response of the ion optics was also measured before and after both the random and sine vibration tests. Presented on Figure 13 is a similar comparison of the data, this time obtained for the ion optics, before (blue) and after (red) the random vibration and after (green) the sine vibration tests. Again, the data show no significant shift in the response indicating that no damage or significant change occurred in the ion optics during both the vibration tests. While only data are presented for the Z axis, very similar data were obtained for both the X and Y axes. From these data, it was concluded that there were no changes in the mechanical characteristics of the thruster as a result of either the random or the sine vibrations tests.

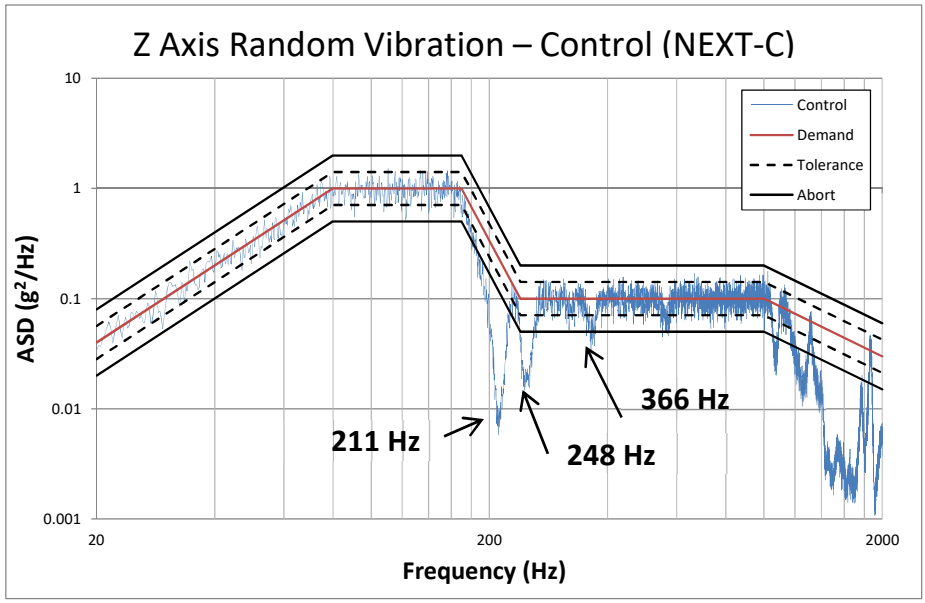

Figure 11 The control accelerometer response for the thruster vibration x axis

For all tests, the input test level was within requirements, natural frequencies were above requirements, and any shifts in natural frequencies were insignificant. Responses for each test were also compared back to a development test performed on a development thruster instrumented similarly to ensure responses were in

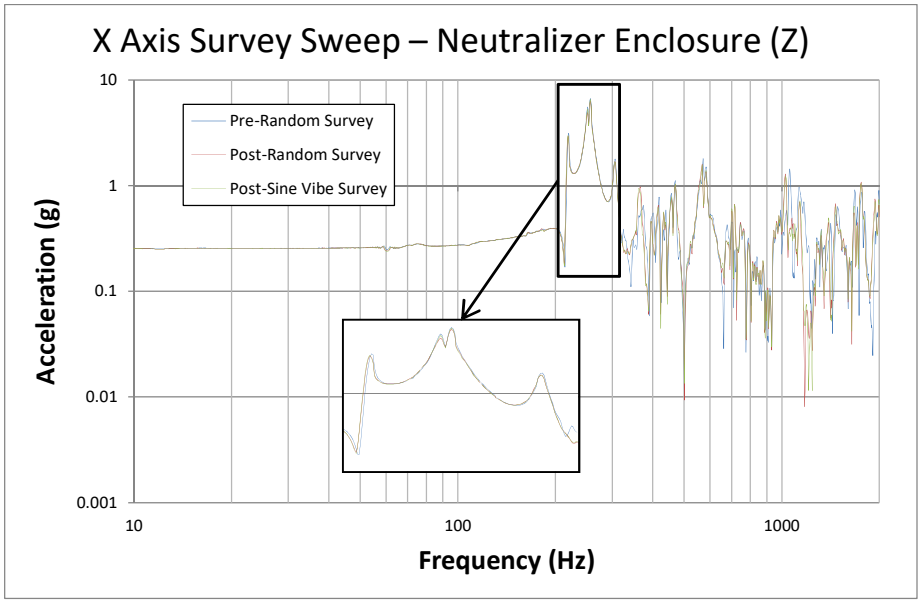

0.3% Neutralizer Frequency Shift

Figure 12 Sine survey results showing that there were negligible shifts in the response of the neutralizer enclosure induced by either the random or sine vibration tests.

family. Finally, visual inspections indicated no damage occurred to the thruster and electrical functional met requirements.

D. Thermal Vacuum Testing

As previously indicated on Figure 6, the flight thruster was subjected to a thermal vacuum test, which is three temperature cycles from the proto-flight cold to hot temperatures. Figure 14 presents the ideal temperature profiles for these three cycles. Specifically the thruster cooled from ambient down to the proto-flight cold temperature at which point it was cold soaked for a minimum of two hours. At the end of the cold soak, as indicated by the solid triangle, the thruster was started and operated in diode mode (TL05 with no beam extraction) for 15 minutes after which the ion beam was extracted and the thruster operated at TL 28. The TL 28 operation continued as the thruster heated up to the proto-flight hot temperature plateau. Once at the hot plateau, the thruster operated at this condition for four hours after which a hot re-start of the thruster was performed.

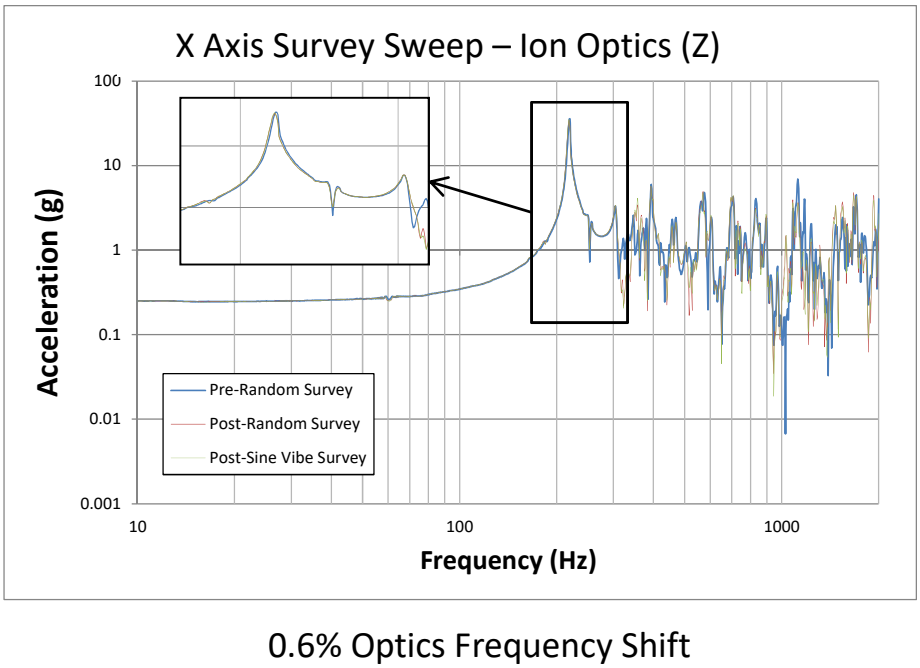

Figure 13 Sine survey results showing that there were negligible shifts in the response of the ion optics induced by the random vibration test.

Figure 15 is a picture of the thruster operating at TL28 as it is actively heated up to the hot temperature plateau using a series of quartz lamps. Presented on Figure 16 is a plot of the three gimbal temperatures as a function of the elapsed time through the first TVAC cycle. As shown, over the night from 0:00 (midnight) to 8:00, the thruster was cooling from-100 °C down to -108 °C. Once the initial cold dwell period elapsed, the thruster was started and the temperature ramp to the hot plateau temperature began.

As the thruster reached the maximum thruster temperature, the 4-hour dwell was begun in which the performance data for the thruster were taken. As mentioned previously, at the completion of the 4-hour dwell, the thruster was

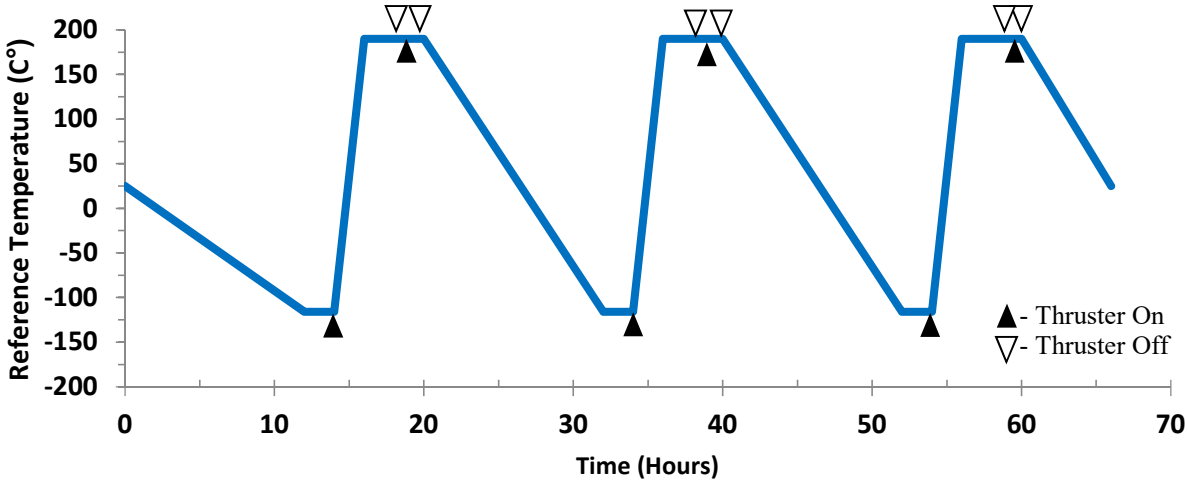

Figure 14 Proto-flight temperature profile showing the temperature extremes tested.

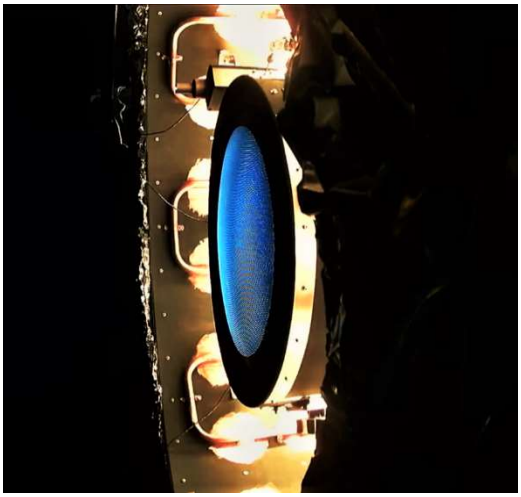

Figure 15 A picture of the flight thruster operating during the heating portion of a thermal vacuum cycle.

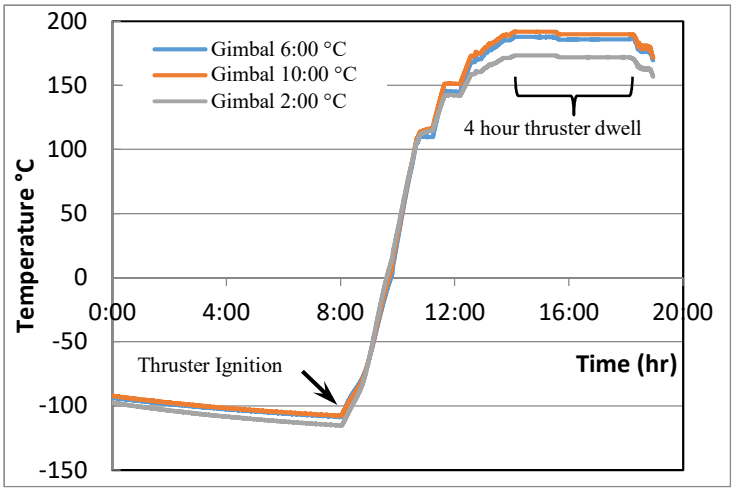

Figure 16 A plot of the three gimbal temperatures for the first TVAC cycle.

turned off and then re-started to demonstrate a hot restart of the thruster. For this first TVAC cycle, after the re-start the thruster was operated in diode mode, i.e. TL05 with no beam extraction, for 15 minutes. At the completion of the hot dwell for the second thermal cycle, a hot re-start of the thruster was performed with the thruster operating at the TL28 discharge conditions and no beam extraction. For the third thermal cycle, at the completion of the hot dwell, the thruster was restarted at TL28 this time with beam extraction.

During each of the six dwell periods, the performance of the thruster was measured to see how the thruster thermal environment affected its operation. A comparison of the data shows that as the temperature increased from TVAC cold to hot, the operating parameters associated with the thruster only varied by a few percent. In addition, recall from Figure 6, the TVAC testing was performed between the two partial functional tests. Hence a comparison of the data presented on Table 5, Table 6, Table 7, and Table 8 shows that the thermal cycling of the thruster did not affect the operation of the thruster.

E. Ion Beam Characteristics

Additionally to document the operation of the flight thruster, data on the ion beam characteristics, (i.e. current density and double to single ion ratio), were measured during the performance and functional tests for each of the throttle levels tested. For the sake of brevity, presented within this paper are only the data obtained for TL28. Figure 17 shows the beam ion current density as a function of radial position through the ion beam. For these data, as mentioned in the experimental apparatus section, the probes were positioned 4.5 cm and 82 cm downstream of the accel grid. At each operating point during a given test (PaT, FuT 1, FuT 2), three data traces were obtained. Shown in Figure 17 are one of the three traces from each separate test. As mentioned previously, the data taken at an axial position of 4.5 cm was taken at a constant axial position while the data taken at 82 cm was obtained as the probe moved on a constant radius arc through the ion beam. Shown on Figure 18 are the ion current density measurements obtained 2.7 m downstream of the thruster as the probe moved on an arc centered at the center of curvature for the optics from one side of the vacuum facility to the other. It should be noted that these data have not been corrected to remove the charge exchange ion current contribution so the data presented contain both the beam and the charge exchange ions. Using the data obtained at the three locations, the contour plot presented on Figure 18 was created. On this figure the blue circles are the actual ion current density measured at each of the three locations and from this data the contour plot shown below the data was generated. Review of the four figures presented shows that near the ion optics, the peak in the current density is very close to the thruster centerline and at the mid-field location, the peak is located 1.6 cm in the minus X direction and at the far field location, the peak in the current density is located

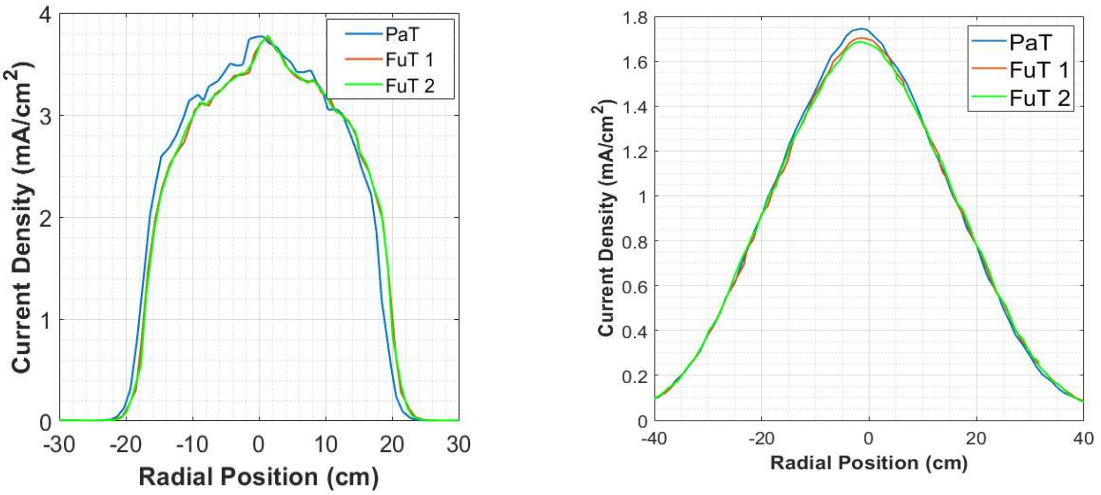

Figure 17 The near and mid field beam current density for TL28. Shown on the figures are the three data traces obtained during the three different performance test (PaT, FuT#1, and FuT#2). The data show the repeatability over the different tests on different days.

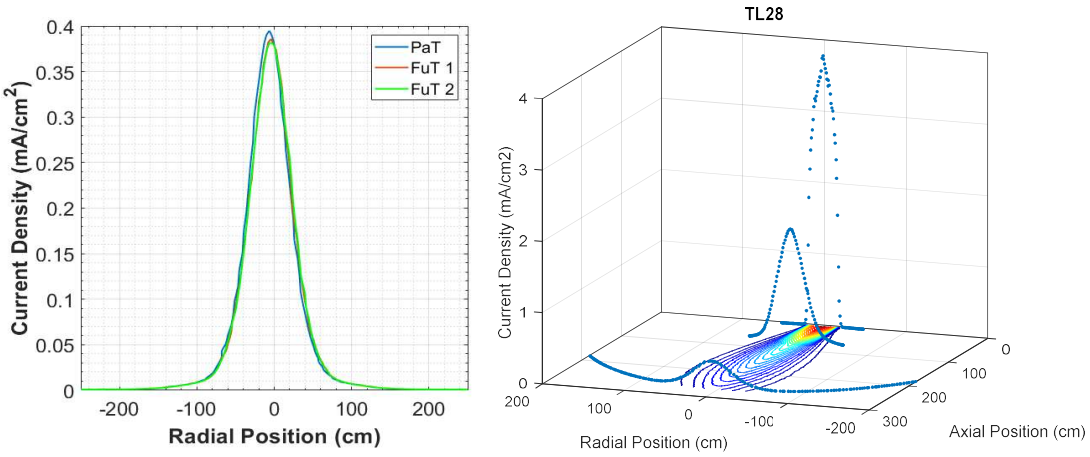

Figure 18 The far field beam ion current density as a function of radial position 2.7 m downstream for the thruster. Using the beam current density data, a contour plot of the current density profiles.

approximately 10 cm in the minus X direction. Using these dimensions suggests that the ion beam is directed approximately 1 to 2 degrees in the X direction which is consistent with the 30 cm (1.4 degree) shift shown on Figure 8 .

In addition to measuring the ion current density profiles downstream of the thruster, an ExB probe was used to measure the ratio of the double to single ions. Identical to the method described by Pollard[8], this spatially-resolved ratio was weighted using the near field beam current density and integrated over the optics area to determine the total double-to-single ion current ratio. This total ratio was then used to calculate thrust. Presented on Figure 19 is a plot of the single ion current and, the double ion current as a function of the probe radial position for TL28. Similar to the

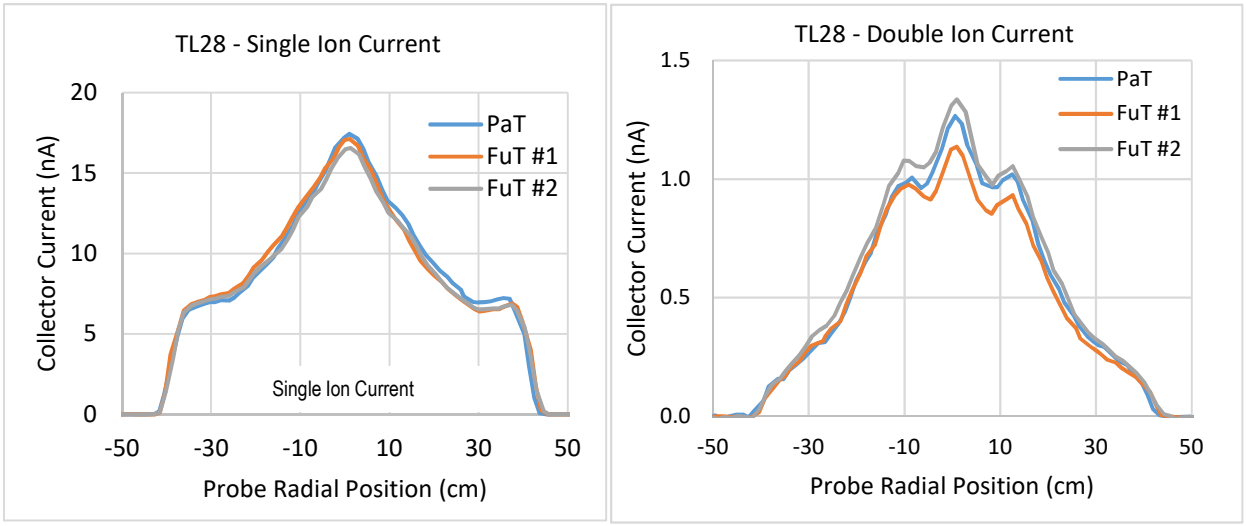

Figure 19 Double, Single ion currents for TL 28 operation measured during the three performance tests.

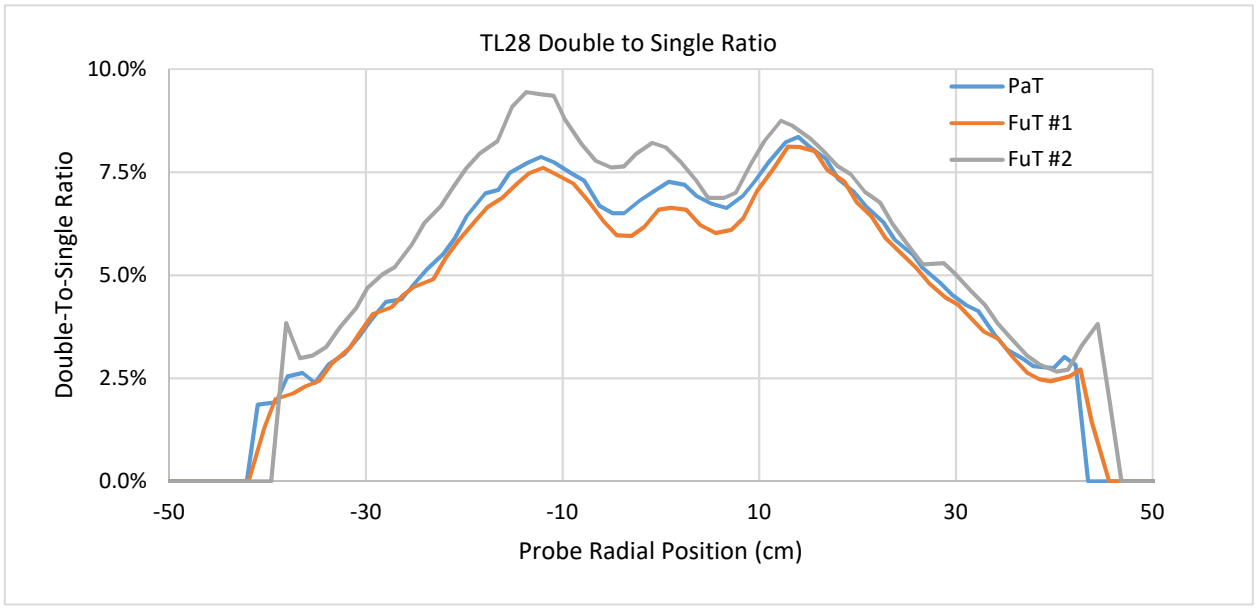

Figure 20 Double-To-Single ratio for TL 28 operation measured during the three performance tests.

previous ion current density plots, these data were also obtained with the thruster operating at TL28 during each of the performance test, PaT, FuT #1, and FuT #2. From the figure, there is a very distinct peak on the centerline located at 2 cm in the X direction which is very similar to the peak in the mid-field current density data. The data for the double ion collector current are less than one tenth of the single ion collector current and interestingly the data show a peak on the centerline and a peak at a radial position of ± 10 cm. This centerline peak and ring in the double ion collector current has been observed before[8] however not to this level of detail. Presented on Figure 20 is the double to single ion current ratio as a function of the probe radial position. These data show that over the central 40 cm of the ion beam, the ratio averages are approximately 7.5% and decline towards the edge of the ion beam.

F. Future Work

Based upon the analysis conducted on the flight design, there are two, minor concerns that may require addressing for future missions. These concerns are both related to the extreme survival temperatures listed in the product specification. Specifically, for the discharge cathode there is a concern that the dissimilar materials in the assembly will fatigue as the cathode thermally cycles from the operational low to high temperatures. In reality, the discharge

cathode assembly will rarely cycle to these operational extreme temperatures, making a fatigue issue unlikely for the majority of missions. A fatigue crack growth analysis can be performed to further gain confidence that this concern will not become an issue for the mission.

The updated thermal analysis also revealed that for the single operating condition of TL37 at proto-flight hot temperatures, the neutralizer and discharge cathode wiring analytically exceed their maximum continuous temperature rating. This exceedance is only for the last few centimeters near the cathodes. Depending upon the mission temperature for future missions, the wire termination design may have to be updated.

All of these potential issues have been documented within in the AR Product Lifecycle Management (PLM) system ensuring that prior to starting the build of a second thruster, they will have to be examined and dispositioned.

VI.Conclusion

Presented within this paper are the results of the proto-flight testing of the SN001 thruster conducted at NASA GRC. The testing involved documenting the performance of the thruster over the NEXT throttle table and comparing those results to previous generations of the design. In addition, tests were conducted to document the thruster performance and show that it did not change throughout the test campaign. The results of these performance measurements showed that the flight thruster was in family with previous NEXT thrusters with the exception of the perveance limits which were slightly lower than prior grid set performance due to a known radial misalignment of the apertures. This testing also showed no changes in the thruster performance as a result of the environmental testing with the exception of a slight shift in the thrust vector location. The new location is still less than the thruster requirement.

The thruster was subjected to a series of environmental tests. Specifically a thermal vacuum test in which it was subjected to three cycles from -110 °C to 190 °C, and proto-flight random and sine vibration tests. For each axis perpendicular to the thrust axis, the thruster was subjected to a level of 15.9 G_{rms}, and in the thrust axis direction, the subjected level was 14.7 G_{rms}. A comparison of the sine survey profiles before and after the vibration testing showed negligible changes in the fundamental frequencies associated with the thruster.

At present, the final inspections of the thruster have been completed, it has been delivered to APL and integrated onto the DART spacecraft.

VII.Endnotes

[1] Patterson, Michael J., et al., "NEXT: NASA's Evolutionary Xenon Thruster," AIAA 2002-3832, 38th AIAA/ASME/SAE/ASEE Joint Propulsion Conference & Exhibit, July 7-10, 2002.

[2] Hoskins, Andrew W., et al., "NEXT Ion Propulsion System Production Readiness," AIAA 2007-5856, 43rd AIAA/ASME/SAE/ASEE Joint Propulsion Conference & Exhibit, July 8-11, 2007.

[3] Van Noord, Jonathan, L., et al., "NEXT PM1R Ion Thruster and Propellant Management System Wear Test Results," IEPC-2009-163, 31st International Electric Propulsion Conference. Sept. 20-24, 2009.

[4] Bontempo, James, J., "The NEXT-C Power Processing Unit: Lessons Learned from the Design, Build, and Test of the NEXT-C PPU for APL's DART Mission," AIAA-2020-3641, AIAA Propulsion and Energy 2020 Forum, August 24-28, 2020.

[5] Reed, C., Cheng, "Asteroid Impact Deflection Assessment: Double Asteroid Redirections Test," IAC-16. A3,4.10,x32340, International Astronautical Federation, Sept. 2016.

[6] Snyder, J.S., et al., "Environmental Testing of the NEXT PM1R Ion Engine," IEPC-2007-276, 30th International Electric Propulsion Conference, Sept. 17-20, 2007.

[7] Patterson, Michael, J., "NEXT Ion Propulsion System Development Status and Performance," AIAA 2007-5199, 43rd AIAA/ASME/SAE/ASEE Joint Propulsion Conference & Exhibit, July 8-11, 2007.

[8] Pollard, James E., et al., "Spatially-Resolved Beam Current and Charge-State Distributions for the NEXT Ion Engine," AIAA 2010-6779, 46th AIAA/ASME/SAE/ASEE Joint Propulsion Conference & Exhibit, July 25-28, 2010.

[9] Polk, J.E., et al., "Behavior of the Thrust Vector in the NSTAR Ion Thruster," AIAA 98-3940, 34th AIAA/ASME/SAE/ASEE Joint Propulsion Conference & Exhibit, July 13-15, 1998.

[10] Fisher, J., et al., "NEXT-C Flight Ion System Status," AIAA-2020-3604, AIAA Propulsion and Energy 2020 Forum, August 24-28, 2020.